A New Procedure for Calculating Immittance Characteristics Using Detailed Computer Simulations

Scott D. Sudhoff, *Senior Member, IEEE*, Benjamin P. Loop, *Student Member, IEEE*, and J. Byoun, *Student Member, IEEE*

***Abstract*— Immittance based methods are often used in the stability analysis of power electronics based systems. Because it is difficult and/or time consuming to develop average value models of some components, it is often desirable to extract immittance data from detailed simulations (simulations in which the switching of the power semiconductors is represented). Traditionally, this is accomplished by introducing a perturbation, extracting the fundamental component of the voltage and current waveforms at the perturbation frequency, from which the impedance at that frequency may be extracted using transform techniques. In this work, an alternate approach is suggested, which offers both reduced computational effort as well as increased accuracy.**

***Index Terms*—Impedance, Impedance measurement, Simulation, Power electronics.**

I. Introduction

IMMITTANCE (impedance or admittance) information of power electronics components is sought for many reasons. One of the main reasons is to evaluate the stability of component interconnections. The use of small signal component immittances to analyze system stability is common [1]–[9]. The method utilized in [1] and [2] involves the concept of "generalized immittance," which is the encapsulated set of all immittances that the component can exhibit over a range of operating points. This approach to stability analysis is dependent upon the ability to calculate immittances accurately and efficiently.

Generalized immittances may be found by several methods. First, immittances can be measured experimentally. This involves introducing a perturbation at a particular frequency into the system, measuring the components of the voltage and current at that frequency, and calculating the magnitude and phase of the impedance or admittance from this data. While a variety of equipment is available to automate this procedure, it requires a significant amount of time and effort.

It is often desirable to calculate component immittances during the design stage. To this end, either a nonlinear average value model (NLAM) [1], [10] or a detailed model (i.e. a model in which the switching of the power semiconductor is represented) may be used. In the case of the nonlinear average value model, immittances are readily calculated by linearization of the model, whereupon the frequency response may be calculated using standard techniques. Unfortunately, there are times when it is difficult to derive a suitable nonlinear average value model. In this case, a detailed simulation can be used to determine component immittances.

The use of a detailed simulation to calculate immittances is considered herein. At first, this may seem to be a straightforward problem. At a given frequency and operating point, a perturbation can be injected whereupon the appropriate voltage and current components can be extracted and used to find the immittance at that frequency and operating point.

Since the time domain simulations employed can require significant computation time (especially since dozens of operating points may be required), it is desirable to introduce a set of perturbations during each simulation, and then use transform techniques to extract the desired components.

A new procedure for decomposing a signal into its frequency components is considered herein. This method is computationally efficient and capable of accurately reproducing time domain waveforms. This method also allows (and requires) harmonics that naturally occur in the system to be represented.

Other methods of signal decomposition are the discrete Fourier transform (DFT), used in [11], and Welch's averaged periodogram method [12], used in [13] (Welch's averaged periodogram method is implemented in the Matlab function 'tfe' [14]). For best results using the DFT to find the impedance at a particular frequency, the time domain data should be truncated to an integer number of cycles of that frequency. Thus, impedance data can only be extracted one frequency at a time. Beating effects between the desired perturbation frequency and low frequency harmonics can prove troublesome.

Welch's averaged periodogram method allows impedances at all perturbation frequencies to be calculated simultaneously, but it does not calculate immittance data precisely at the perturbation frequencies. Instead, data at frequencies near the perturbation frequencies must be accepted. This can prove troublesome when conducting generalized immittance analysis wherein the immittance at prescribed frequencies is desired.

This work was supported by the "Naval Combat Survivability" effort, Grant N00024-02-NR-60427.

S. D. Sudhoff and B. P. Loop are with Purdue University, West Lafayette, IN 47907 USA (phone: 765-494-3487; fax: 765-494-0676; e-mail: loop@ieee.org).

J. Byoun is with the University of Illinois, Urbana-Champaign, IL, USA

A three-way comparison among the DFT, Welch's averaged periodogram method and the proposed method demonstrates that all three methods can yield acceptable results. The proposed approach, however, allows the user to specify precisely the frequencies for which immittances are calculated and simultaneously calculate the immittances of all frequencies of interest.

II. GENERAL APPROACH

The source-load system shown in Fig. 1 will be used for a basis of discussion for the proposed techniques. Therein, the voltages across the source and load are denoted v_s and v_l, respectively. The current from the source to load is labeled i_{sl}. Finally, the perturbation source is an ideal voltage source whose instantaneous voltage is denoted v_p.

The basic goal is to perform a detailed simulation study which will provide enough information to extract the small-signal immittances at a desired set of frequencies. In a physical system, the perturbation source will often be at a single frequency in order to achieve the highest possible signal-to-noise ratio. However, when using detailed computer simulations (which are much less noisy than physical systems, even when switching is represented) it is possible to simultaneously inject all frequencies of interest at one time, so that only one study is needed to obtain the entire frequency response. To this end, the perturbation voltage will be of the form

$$v_p = \sum_{n=1}^{N} v_{p,i} \cos\left(\theta_{p,i}\right), \tag{1}$$

where

$$\theta_{p,i} = \omega_{p,i} t + \phi_{p,i}\,. \tag{2}$$

The set of $\omega_{p,i}$ defines the frequencies at which immitances are sought. These frequencies will often be logarithmically distributed over some range. The selection of the perturbation amplitudes clearly requires a degree of engineering judgment; this will be addressed in the case study in Section VII.

One of the principal advantages of the proposed technique is that the perturbation energy can be arbitrarily distributed, and that the extraction process can focus on and take advantage of prior knowledge of the perturbation and switching ripple frequencies. Using transform techniques, the reconstruction frequencies are set by the sampling time.

III. WAVEFORM REPRESENTATION

In order to set forth the proposed method of impedance extraction, it is convenient to first set forth some definitions related to waveform representation. The first of these is an

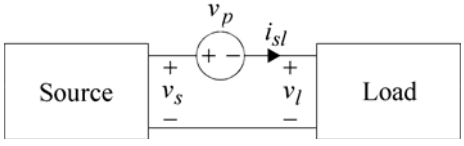

Fig. 1. Source Load System.

angle vector $\boldsymbol{\theta}(t)$ that consist of N angular components organized in a row vector as

$$\boldsymbol{\theta}(t) = \left[\theta_1(t) \quad \theta_2(t) \quad \cdots \quad \theta_N(t)\right]. \tag{3}$$

Often, the individual components will be of the form

$$\theta_n(t) = \omega_n t + \theta_{0n}\,, \tag{4}$$

where $n \in \left[1 \cdots N\right]$, and where ω_n and θ_{0n} represent the angular radian frequency and initial value of the n'th component. Note that (4) is a typical form; not a defining form.

Herein, it will be attempted to approximate a signal $f(t)$ in the form

$$f_{apr}(t) = f_{dc} + \mathbf{C}(\boldsymbol{\theta}(t))\mathbf{f}_c + \mathbf{S}(\boldsymbol{\theta}(t))\mathbf{f}_s\,, \tag{5}$$

where f_{dc} represents and average value, $\mathbf{f}_c$ and $\mathbf{f}_s$ are constant coefficient vectors in $\Re^N$, and $\mathbf{C}$ and $\mathbf{S}$ are matrix valued function in general (but are vector valued functions in (5)) whose elements are given by

$$\mathbf{C}_{i,j}(\boldsymbol{\alpha}) = \cos(\boldsymbol{\alpha}_{i,j}) \tag{6}$$

and

$$\mathbf{S}_{i,j}(\boldsymbol{\alpha}) = \sin\left(\boldsymbol{\alpha}_{i,j}\right), \tag{7}$$

where $\boldsymbol{\alpha}$ is a dummy matrix variable and i and j are arbitrary indices. Physically, f (and coefficients f_{dc}, $\mathbf{f}_c$, and $\mathbf{f}_s$) could represent voltages, currents, or any other signal of interest.

The representation (5) is quite flexible. In some ways, it is reminiscent of a truncated Fourier series. However, whereas a truncated Fourier series is restricted to representing periodic function, the representation of (5) is not. This is because the frequencies of the angle vectors need not be related in a rational way. Clearly, not every signal can be represented in the form of (5); however, this form will be shown to be adequate for the application at hand.

IV. WAVEFORM ESTIMATION – PART I

In this section, it is supposed that a signal $f(t)$ is given and that is desired to calculate parameters f_{dc}, $\mathbf{f}_c$, and $\mathbf{f}_s$. To do this, the waveform $f(t)$ will be sampled at M times, where

$$M \geq 2N + 1\,. \tag{8}$$

The time of the m'th sample is denoted t_m. Thus,

$$f(t_m) = f_{apr}(t_m)\,. \tag{9}$$

From (5), at time t_m

$$f(t_m) = \left[1 \quad \mathbf{C}(\boldsymbol{\theta}(t_m)) \quad \mathbf{S}(\boldsymbol{\theta}(t_m))\right]\begin{bmatrix} f_{dc} \\ \mathbf{f}_c \\ \mathbf{f}_s \end{bmatrix}. \tag{10}$$

Using (10) to formulate an expression for the m'th row. Equation (5) is of the form

$$\mathbf{A}\mathbf{x} = \mathbf{b}\,, \tag{11}$$

where

$$\mathbf{A} = \left[\mathbf{1}_{M\times 1} \quad \mathbf{C}(\boldsymbol{\Theta}) \quad \mathbf{S}(\boldsymbol{\Theta})\right], \tag{12}$$

$$\mathbf{b} = \left[f(t_1) \quad f(t_2) \quad \cdots \quad f(t_M)\right]^T, \tag{13}$$

and

$$\mathbf{x} = \begin{bmatrix} f_{dc} & \mathbf{f}_c^T & \mathbf{f}_s^T \end{bmatrix}^T . \quad (14)$$

In (12),

$$\mathbf{\Theta}_{m,n} = \theta_n(t_m) . \quad (15)$$

The least squares fit solution to (11) is given by

$$\mathbf{x} = \left(\mathbf{A}^T\mathbf{A}\right)^{-1}\mathbf{A}^T\mathbf{b} . \quad (16)$$

V. Waveform Estimation – Part II

In many cases, it will be found that (5) cannot be used to accurately represent the waveform, because of the presence of high-frequency switching ripple. In this case, it is appropriate to represent not the instantaneous waveform, but rather its filtered value. To this end, the filtered waveform will be given in the time domain by

$$\overline{x}(t) = \int_{-\infty}^{t} x(\lambda)h(t-\lambda)d\lambda , \quad (17)$$

where $h(t)$ is the impulse response of the filter (which is typically either low pass or bandpass). As $t \to \infty$, the filtered approximation the waveform is given by

$$\overline{f_{apr}}(t) = H_{dc} f_{dc} + \overline{\mathbf{C}}(\mathbf{\theta}(t))\mathbf{f}_c + \overline{\mathbf{S}}(\mathbf{\theta}(t))\mathbf{f}_s \quad (18)$$

where H_{dc} is the dc gain of the filter and where

$$\overline{\mathbf{C}_{ij}}(t) = \int_{-\infty}^{t} \cos(\alpha_{ij}(\lambda))\, h_{lpf}(t-\lambda)d\lambda \quad (19)$$

and

$$\overline{\mathbf{S}_{ij}}(t) = \int_{-\infty}^{t} \sin(\alpha_{ij}(\lambda))\, h_{lpf}(t-\lambda)d\lambda . \quad (20)$$

It should be noted that while (19) – (20) provide a definition, $\overline{\mathbf{C}}$ and $\overline{\mathbf{S}}$ can be readily calculated analytically using phasor analysis. Setting the filtered waveform equal to the filtered approximation to the waveform at M sample times yields a linear system of equations of the form (11), where

$$\mathbf{A} = \left[\mathbf{1}_{M\times 1} H_{dc} \quad \overline{\mathbf{C}}(\mathbf{\Theta}) \quad \overline{\mathbf{S}}(\mathbf{\Theta})\right], \quad (21)$$

$$\mathbf{x} = \begin{bmatrix} f_{dc}H_{dc} & \mathbf{f}_c^T & \mathbf{f}_s^T \end{bmatrix}^T , \quad (22)$$

and

$$\mathbf{b} = \begin{bmatrix} \overline{f_{sm}}(t_1) & \overline{f_{sm}}(t_2) & \cdots & \overline{f_{sm}}(t_M) \end{bmatrix}^T , \quad (23)$$

which is readily solved for the coefficients using (16). If H_{dc} is zero (i.e. a bandpass rather than a lowpass filter is used), then $\mathbf{A}$ and $\mathbf{x}$ become

$$\mathbf{A} = \left[\overline{\mathbf{C}}(\mathbf{\Theta}) \quad \overline{\mathbf{S}}(\mathbf{\Theta})\right] \quad (24)$$

and

$$\mathbf{x} = \begin{bmatrix} \mathbf{f}_c^T & \mathbf{f}_s^T \end{bmatrix}^T . \quad (25)$$

VI. IMMITTANCE MEASUREMENT

The procedure whereby this method of signal extraction can be used to calculate immittance characteristics is now set forth. To this end, it is appropriate to partition the angle vector $\mathbf{\theta}$ as

$$\mathbf{\theta} = \left[\mathbf{\theta}_r \quad \mathbf{\theta}_p\right] \quad (26)$$

where $\mathbf{\theta}_r$ is a vector of angular positions whose corresponding frequencies are the power electronics ripple frequencies that are within the band pass of the filter. The vector $\mathbf{\theta}_p$ is the vector of angular positions corresponding to perturbation frequencies (see (1)). It is convenient to partition $\mathbf{f}_c$ and $\mathbf{f}_s$ the same way, i.e.,

$$\mathbf{f}_c^T = \left[\mathbf{f}_{cr}^T \quad \mathbf{f}_{cp}^T\right] \quad (27)$$

and

$$\mathbf{f}_s^T = \left[\mathbf{f}_{sr}^T \quad \mathbf{f}_{sp}^T\right]. \quad (28)$$

Next, each variable of interest is decomposed using the procedure of Section IV. The phasor representation of the signal at the i'th perturbation frequency is given by

$$\tilde{f}_i = f_{cp,i} - jf_{sp,i} , \quad (29)$$

where $f_{cp,i}$ and $f_{sp,i}$ are the i'th components of $\mathbf{f}_{cp}$ and $\mathbf{f}_{sp}$ respectively, and where $j = \sqrt{-1}$. If an impedance is sought, then the impedance at the i'th frequency may be readily expressed

$$z_i = \frac{\tilde{v}_i}{\tilde{i}_i} . \quad (30)$$

VII. Case Study: Inverter Module

The proposed approach is now applied to an inverter module used to supply an ac bus from a dc source. The inverter module consists of an input capacitor, a fully controlled bridge converter, an LC filter, and control algorithms. This section contains a description of the inverter module and a comparison of the admittance calculated with the proposed approach, the admittance calculated using the DFT and Welch's averaged periodogram methods, and the admittance measured experimentally.

A. Inverter Module Description

The entire inverter module is depicted in Fig. 2, and the LC filter is depicted in Fig. 3. Note that parasitic resistances the inductors and capacitors are modeled. Parameter values for the physical components are listed in Table I, which can be found in the Appendix. Note that in the diagram in Fig. 2, measured quantities are differentiated from actual physical quantities. For instance, the actual a-phase current into the LC filter is i_{aL}, whereas the measurement of this quantity is denoted as $\hat{i}_{aL}$. The same notation is used for the output currents, i_{aO} and i_{bO}, and the output line to line voltages, v_{abO} and v_{cbO}.

The inverter module is controlled so that it appears as a voltage source. The control is broken into three stages. The first stage, depicted in Fig. 4, generates the commanded values for the currents out of the bridge so that the desired output voltages are obtained. The first step in this control is to transform the measured output line to line voltage, $\hat{v}_{abO}$ and

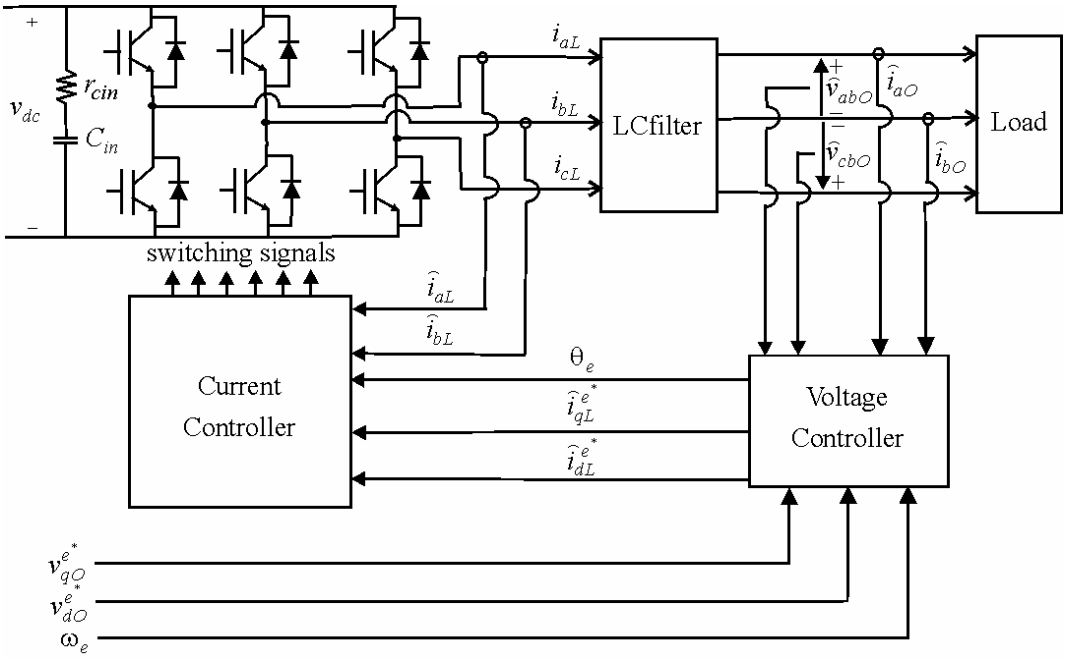

Fig. 2. Diagram of inverter module

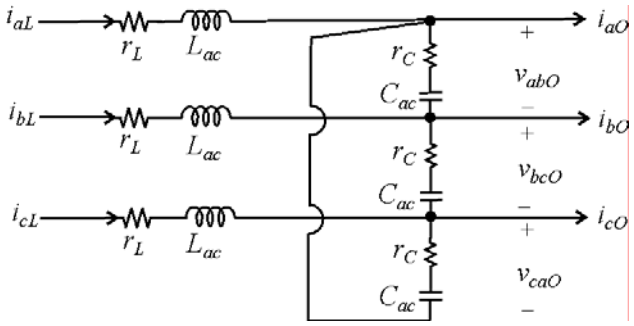

Fig. 3. LC Filter

$\hat{v}_{cbO}$, into a reference frame that varies with θ_e, the desired angular position of the inverter output waveforms.

More specifically, this transformation is

$$\begin{bmatrix} \hat{v}_{qO}^{e} \\ \hat{v}_{dO}^{e} \end{bmatrix} = \mathbf{K}_v^e \begin{bmatrix} \hat{v}_{abO} \\ \hat{v}_{cbO} \end{bmatrix} = \frac{2}{3}\begin{bmatrix} \cos(\theta_e) & -\cos(\theta_e + 2\pi/3) \\ \sin(\theta_e) & -\sin(\theta_e + 2\pi/3) \end{bmatrix} \begin{bmatrix} \hat{v}_{abO} \\ \hat{v}_{cbO} \end{bmatrix}. \tag{31}$$

Note that this transformation assumes that the load is wye connected. The measured currents are also transformed to the synchronous reference frame using

$$\begin{bmatrix} \hat{i}_{qO} \\ \hat{i}_{dO} \end{bmatrix} = \mathbf{K}_i^e \begin{bmatrix} \hat{i}_{aO} \\ \hat{i}_{bO} \end{bmatrix} = \frac{2}{\sqrt{3}}\begin{bmatrix} \cos(\theta_e - \pi/6) & \sin(\theta_e) \\ \sin(\theta_e - \pi/6) & -\cos(\theta_e) \end{bmatrix} \begin{bmatrix} \hat{i}_{aO} \\ \hat{i}_{bO} \end{bmatrix}. \tag{32}$$

A decoupling feedback is implemented using the speed of the inverter reference frame, ω_e, and the estimated wye-equivalent filter capacitance, $C_{eq,est}$. A proportional plus integral controller acts on the difference between the commanded q- and d-axis voltages, v_{qO}^{e*} and v_{dO}^{e*}, and the measured q- and d-axis voltages to generate signals that either increase or decrease the commanded q- and d-axis current commands. The q- and d-axis current commands, $\hat{i}_{qL}^{e*}$ and $\hat{i}_{dL}^{e*}$, are then passed through a current limiter to prevent excessive current levels. This control was first set forth in [15].

The second stage of the control is the synchronous current regulator [16]. A diagram of this control is depicted in Fig. 5. Note that in this figure, the following vector notation is used:

$$\mathbf{i}_{qdL}^{e*} = \begin{bmatrix} i_{qL}^{e*} & i_{dL}^{e*} \end{bmatrix}^T \tag{33}$$

and

$$\mathbf{i}_{abcL}^{*} = \begin{bmatrix} i_{aL}^{*} & i_{bL}^{*} & i_{cL}^{*} \end{bmatrix}^T. \tag{34}$$

This control guarantees that the desired fundamental component of the current waveform is achieved if sufficient voltage is available. The synchronous current regulator is essentially a proportional plus integral control acting on the difference between the q- and d- axis commanded and actual currents in the LC filter inductors. Note that the same reference frame transformation used in (32) is used to transform the measured inductor currents to the synchronous reference frame. The modified q- and d-axis current commands, i_{qdL}^{e**} and i_{dL}^{e**}, are converted to a-, b-, and c-phase current commands using

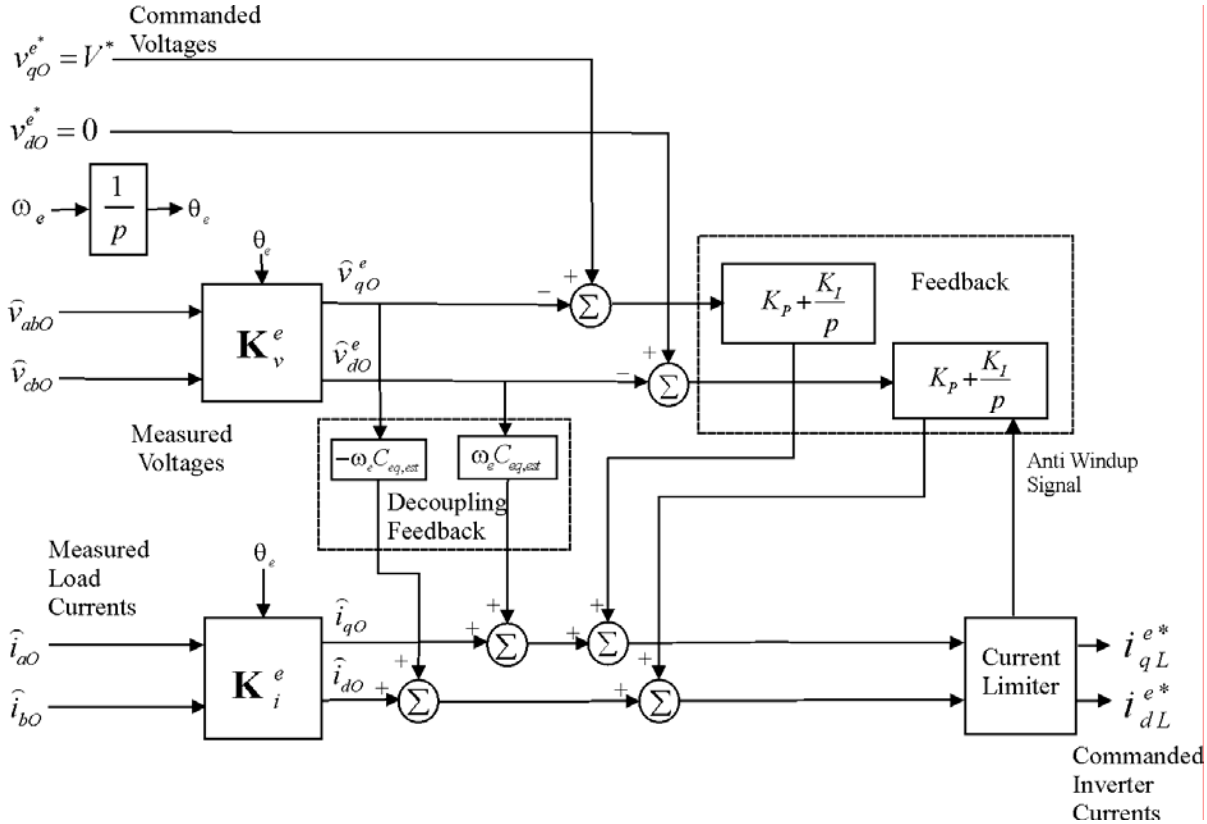

Fig. 4. Inverter module voltage regulator

$$\begin{bmatrix} i_{aL}^{*} \\ i_{bL}^{*} \\ i_{cL}^{*} \end{bmatrix} = \mathbf{K}_s^{e\,-1}\Big|_{ltc} \begin{bmatrix} i_{qL}^{e**} \\ i_{dL}^{e**} \end{bmatrix} = \begin{bmatrix} \cos(\theta_e) & \sin(\theta_e) \\ \cos(\theta_e - 2\pi/3) & \sin(\theta_e - 2\pi/3) \\ \cos(\theta_e + 2\pi/3) & \sin(\theta_e + 2\pi/3) \end{bmatrix} \begin{bmatrix} i_{qL}^{e**} \\ i_{dL}^{e**} \end{bmatrix} \tag{35}$$

The last stage of the control is a hysteretic-delta modulator. This modulator generates the switching signals for the transistors in the inverter based on the current commands given by the synchronous current regulator. The hysteretic-delta modulator is a combination of the hysteresis and the delta modulators [17]. The diagram in Fig. 6 depicts a state transition diagram for the 'x' leg of the inverter module using the hysteretic delta modulator (x can be a, b, or c). There are two states in this diagram. The first represents allowing the upper switch in the 'x' leg to conduct and preventing the lower switch from conducting. The second represents the opposite. The condition for a transition is tested periodically with frequency f_{sample}. When the condition is true, the state is changed. Staggered switching is used. That is, the condition for the state of the switches in phase b to change is checked $1/(3f_{sample})$ after phase a, and phase c is checked $1/(3f_{sample})$ after phase b and so on. This prevents any two phase legs from switching at the same time and thereby reduces the effects of electromagnetic interference. This modulator allows direct limitation of the switching frequency

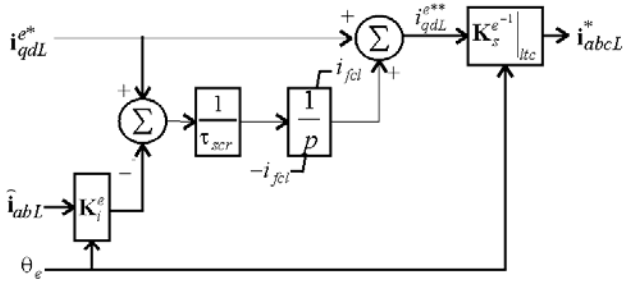

Fig. 5. Synchronous current regulator

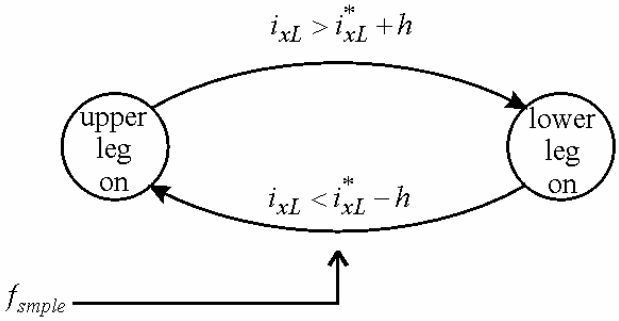

Fig. 6. Hysteretic delta modulator

of each leg and also gives a measure of control of the fidelity of the signal through the hysteresis level, h. Control parameters are listed in Table II in the Appendix.

B. Admittance Measurement and Comparison

A time domain simulation of the inverter module was developed and used to conduct the proposed admittance measurement technique.

The first study, depicted in Fig. 7, is the small signal admittance when the inverter module input dc voltage is 420 V and the output power is 9.6 kW. Admittances were measured at 30 frequencies logarithmically spaced between 10 Hz and 10 kHz using the procedure described above. For this study, three cascaded first-order low pass filters with cut-off frequency of 5 kHz were used. The perturbation voltage magnitudes for all of these frequencies were set to 0.5 V. The selection of the magnitude of the voltage perturbation requires some engineering judgment. It should not be so big that it severely affects the performance of the device under investigation. The reduced noise in a computer simulation compared to experimental test set-ups allows the use of smaller perturbations. The admittance was also measured experimentally by introducing a perturbation at a single frequency with a transformer. The admittance at that frequency was then measured and calculated with a Hewlett Packard 35650 network analyzer. The admittance measured using time domain simulation and the admittance measured experimentally on a hardware test system are depicted. As can be seen, the proposed method accurately predicts the observed admittance.

The validity of the procedure depends on its ability to recreate the time domain voltage or current data. The voltage and current simulation waveforms and reconstructed waveforms are depicted in Fig. 8. Note that a small offset was added to the reconstructed waveforms so they could be differentiated from the original in the plot. The procedure does indeed recreate the waveforms accurately.

The admittance prediction of the proposed approach is now compared to other possible procedures. The first alternate approach is to use the DFT. Identical voltage and current data used with the proposed approach can be used with the DFT (i.e. filtered data with perturbations at many frequencies simultaneously). For each of the perturbation frequencies, the data is truncated so that it includes the largest integer number of cycles of that frequency. Then the DFT is applied to the truncated data and the voltage, $\tilde{v}_i$, and current component, $\tilde{i}_i$, at the frequency is extracted. Then, (30) can be applied to calculate admittance. The results of this analysis are depicted in Fig. 9.

A second alternate approach is to use Welch's averaged periodogram method. This was applied to the same voltage and current data used with both the DFT and proposed approaches. This method performs frequency analysis on a number of subsections of the data, and then averages the results together to calculate frequency domain information for the entire set of data. The results are dependent upon the number of subsections analyzed and averaged. Finding the best number of subsections to use by trial and error can be tedious and time consuming. The frequency domain data returned by the procedure does not correspond precisely to the actual perturbation frequencies. Thus, the analyst must use data corresponding to frequencies close to the perturbation frequencies. The rest of the data corresponds to other frequencies and is meaningless with regard to immittance computation. It should, therefore, be disregarded. The results of this analysis are depicted in Fig. 10.

The predictions of the proposed approach are compatible

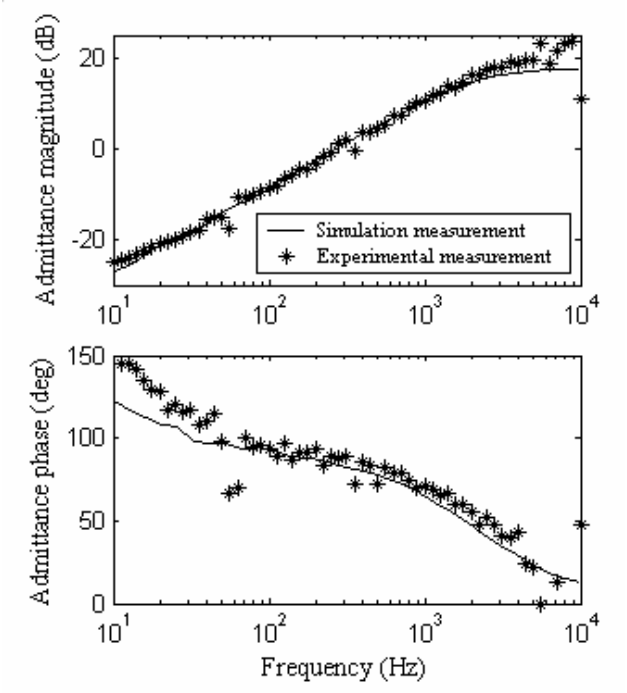

Fig. 7. Admittance measurement using proposed approach

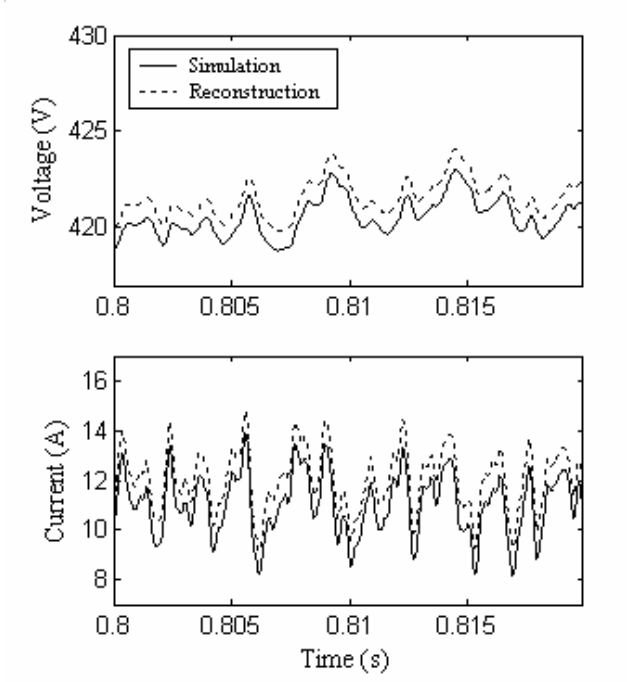

Fig. 8. Waveform reconstruction comparison

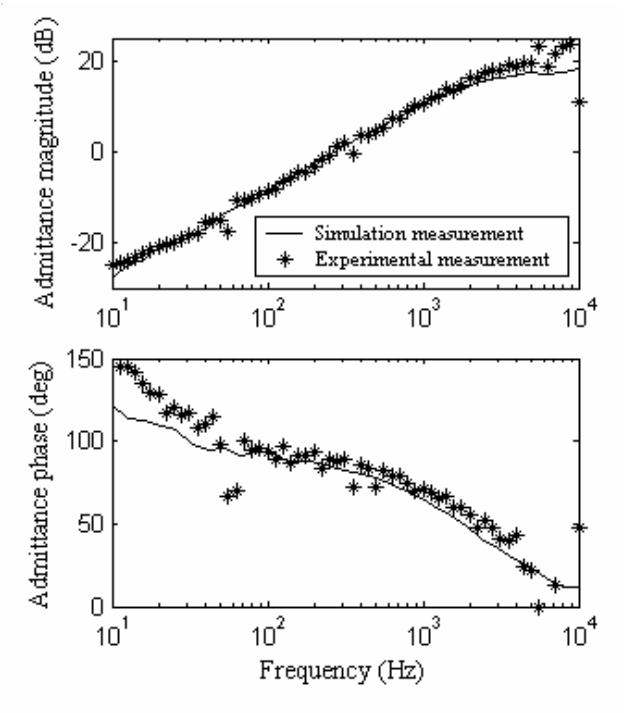

Fig. 9. Admittance measurement using DFT

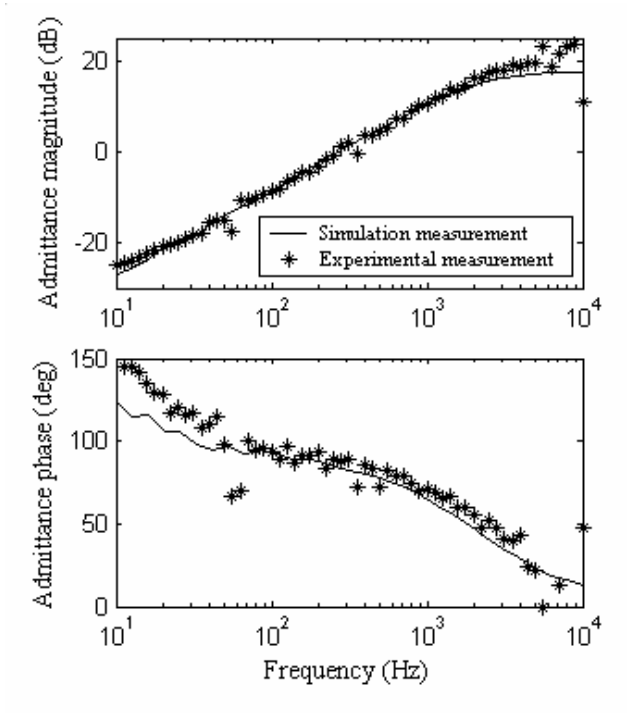

Fig. 10. Admittance measurement using Welch's averaged periodogram method

with those of the other two approaches. Advantages of the proposed method include the ability to specify the precise frequencies for which immittance data is desired, to calculate the immittance at all perturbation frequencies simultaneously and to use knowledge of frequencies that occur naturally in the system to increase accuracy.

C. Generalized Admittance

The stability analysis technique developed in [1] and [2] utilizes the concept of a generalized admittance. In general, small signal admittances of nonlinear power system components can only be evaluated at a particular operating point. A generalized admittance, on the other hand, is the encapsulated set of all admittances that the component can exhibit over a range of operating points. For example, Fig. 11 depicts the generalized admittance of the inverter module, measured experimentally, for a family of operating points. This family is all combinations of input dc voltage and output power, where the input dc voltage is allowed to assume either 400 V or 420 V, and the output power is allowed to assume 0 W, 4.6 kW, or 9.6 kW. The sudden widening of the generalized admittance in the 60 Hz region is due to undesirable parasitic coupling to the laboratory power system. The widening of the admittance at high frequencies is due to the switching of the power electronics converters, which degrades the admittance measurement. Fig. 12 depicts the generalized admittance for the same family of operating points measured using time domain simulations. The generalized admittance measured with time domain simulations closely matches the experimentally measured generalized admittance.

VIII. CONCLUSIONS

A novel method of calculating the immittance of a power electronics based system component was set forth. This method is based on detailed simulations and can, therefore, be used in the design process even for converters/controls wherein it is too difficult to derive an average value model. It is computationally efficient since immittance values can be calculated at many frequencies simultaneously. The results of a case study show that the method can accurately calculate immittances and the underlying waveform representation scheme is capable of encapsulating the harmonic content of signals. The alternate approaches of using the DFT or Welch's averaged periodogram method were shown to obtain similar results, however, these methods have the disadvantages of requiring the time-domain to be truncated on a frequency-by-frequency basis (DFT) or not calculating the immittance at the perturbation frequencies (Welch's method).

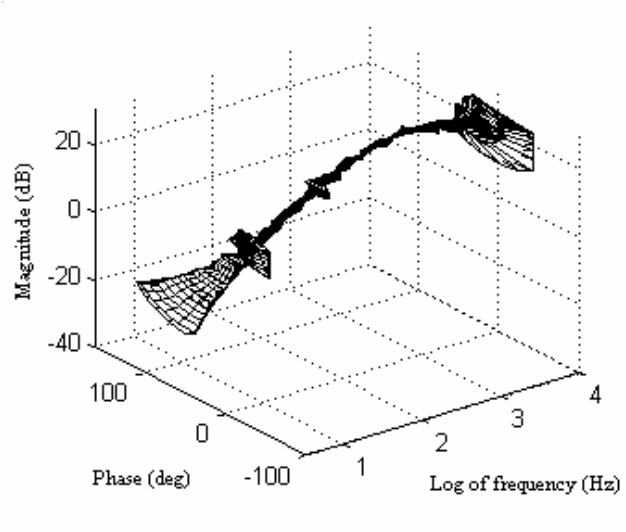

Fig. 11. Generalized admittance measured experimentally.

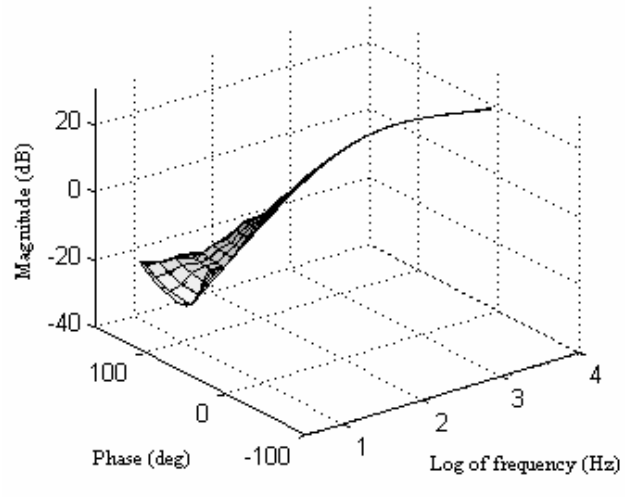

Fig. 12. Generalized admittance measured using the proposed approach.

APPENDIX
INVERTER MODULE AND CONTROL PARAMETERS

TABLE I.
INVERTER PARAMETERS

Symbol	Description	Value
v_{sw}	Controlled switch voltage drop	2 V
r_{sw}	Controlled switch resistance	10 mΩ
v_d	Diode voltage drop	2 V
r_d	Diode resistance	10 mΩ
C_{in}	Input capacitance	590 μ F
r_{Cin}	Input capacitor series resistance	127 mΩ
L_{ac}	Filter inductor inductance	550 μH
r_L	Filter inductor resistance	38 mΩ
C_{ac}	Filter capacitor capacitance	50 μF
r_C	Filter capacitor series resistance	8 mΩ

TABLE II.
CONTROL PARAMETERS

Symbol	Description	Value
$C_{eq,est}$	Estimated wye-equivalent filter capacitance	150 μF
K_p	Proportional feedback gain	225 mA/V
K_i	Integral feedback gain	46.9 mA/(Vs)
i_{limit}	Current limit	50 A
τ_{scr}	SCR time constant	0.5 ms
i_{fcl}	Feedback current limit	20 A
f_{smple}	Per-phase sampling frequency for hysteretic-delta modulator	100 kHz
h	Hysteresis level for hd modulator	1.5 A

REFERENCES

[1] S. D. Sudhoff and S. F. Glover, "Modeling techniques, stability analysis, and design criteria for dc power systems with experimental validation," *1998 Society of Automotive Engineers Transactions, Journal of Aerospace*, pp. 52-67.

[2] S. Sudhoff and S. Glover, "Three-dimensional stability analysis of dc power electronics based systems," *Power Electronics Specialists Conference*, Vol. 1, pp. 101-106, June 2000.

[3] F. Le Magoarou and F. Monteil, "Influence of the load characteristics and the line impedance on the stability of an active power filter," Fifth International Conference on Power Electronics and Variable-Speed Drives, pp. 175-180, Oct 1994.

[4] A. Emadi and M. Ehsani, "Negative impedance stabilizing controls for pwm dc-dc converters using feedback linearization techniques," 35th Intersociety Energy Conversion Engineers Conference and Exhibit, vol. 1, pp. 613-620, Jul 2000.

[5] C. M. Wildrick, F. C. Lee, B. H. Cho, and B. Choi, "A method of defining the load impedance specification for a stable distributed power system," *IEEE Transactions on Power Electronics*, vol. 10, issue 3, pp. 280-285, May 1995

[6] X. Feng, J. Liu, and F. C. Lee, "Impedance specifications for stable dc distributed power systems," *IEEE Transactions on Power Electronics*, vol. 17, issue 2, pp. 157-162, Mar 2002.

[7] D. L. Logue and P. T. Krein, "Preventing instability in dc distribution systems by using power buffering," 32nd Annual Power Electronics Specialists Conference, vol. 1, pp. 33-37, Jun 2001.

[8] K. Smith and L. Ran, "Voltage stability assessment of isolated power systems with power electronic converters," *IEE Proceedings on Generation, Transmission, and Distribution*, vol. 141, pp. 310-314, July 1994.

[9] L. Bohmann and H. Feng, "Small signal transient stability of periodically switched circuits," *Proceedings of the 37th Midwest Symposium on Circuits and Systems*, vol. 2, pp. 1299-1302, Aug. 1994.

[10] S. Sanders and G. Verghese, "Synthesis of averaged circuit models for switched power converters," *IEEE International Symposium on Circuits and Systemes*, Vol. 1, pp. 679-683, May 1990.

[11] B. Palethorpe, M. Sumner, and D. W. P. Thomas, "System Impedance measurement for Use with Active Filter Control," *IEEE Power Electronics Specialists Conference 2001*, Vol. 2, pp. 522-527, June 2001.

[12] G. Zelniker and F. Taylor, *Advanced Digital Signal Processing – Theory and Applications*, New York, NY: Marcel Dekker, Inc. 1994.

[13] M. Sumner, B. Palethorpe, D. W. P. Thomas, P. Zanchetta, and M. C. Di Piazza, "A technique for power supply Harmonic impedance estimation using a controlled voltage disturbance," *IEEE Transactions on Power Electronics*, Vol. 17, Issue 2, pp. 207-215, March 2002.

[14] The Math Works, Inc. *Using Matlab*, Natick, MA, 2002.

[15] O. Wasynczuk, S. D. Sudhoff, T. D. Tran, D. H. Clayton, and H. J. Hegner, "A voltage control strategy for current-regulated pwm inverters," *IEEE Transactions on Power Electronics*, vol. 11, no. 1, pp. 7-15, Jan 1996.

[16] T. M. Rowan and R. J. Kerkman, "A new synchronous current regulator and an analysis of current-regulated pwm inverters," *IEEE Transactions on Industry Applications*, vol. IA-22, no. 4, pp. 678-690, July/Aug 1986.

[17] P. C. Krause, O. Wasynczuk, and S. D. Sudhoff, *Analysis of Electric Machinery and Drive Systems*, New York, NY: John Wiley and Sons, Inc., 2001.

Scott D. Sudhoff received the B.S. (highest distinction), M.S., and Ph.D. degrees in electrical engineering from Purdue University in 1988, 1989, and 1991, respectively. From 1991-1993, he served as visiting faculty with Purdue University. From 1993 to 1997, he served as a faculty member at the University of Missouri - Rolla, and in 1997 he joined the faculty of Purdue University, where he currently holds the rank of Full Professor. His interests include electric machines, power electronics, finite-inertia power systems, applied control, and genetic algorithms. He has published over forty journal papers, including four prize papers, in these areas.

Benjamin P. Loop is a Ph.D. student at Purdue University. He received his B.S. (highest distinction) and M.S. in electrical engineering from Purdue University in 2000 and 2002 respectively. His interests include electric machines, power electronics, applied control, genetic algorithms and nonlinear dynamic systems.

Jaesoo Byoun is a Ph.D. student at University of Illinois at Urbana-Champaign. He received his B.S. from Soongsil University in Seoul, Korea and M.S. from Purdue University both in electrical engineering in 1999 and 2001 respectively. His interests include digital control analysis in power electronics, portable power management control circuit and its algorithm.